Vol.3, No.5, 401-407 (2011)
http://dx.doi.org/10.4236/ns.2011.35054

Natural Science

Design of supercontinuum generating photonic crystal fiber at 1.06, 1.31 and 1.55 μm wavelengths for medical imaging and optical transmission systems

Feroza Begum*, Yoshinori Namihira

Graduate School of Engineering and Science, University of the Ryukyus, Okinawa, Japan; *Corresponding Author:
feroza1972@yahoo.com

Received 29 March 2011; revised 14 April 2011; accepted 20 April 2011.

ABSTRACT

We propose broad supercontinuum spectrum generating highly nonlinear photonic crystal fiber (HN-PCF) which can be used in ultrahigh-resolution optical coherence tomography and optical transmission systems. Using full vector finite difference method, we investigated the different properties of HN-PCF. Broadband supercontinuum spectrum is numerically calculated by using nonlinear Schrödinger equation. Investigation showed that it is possible to obtain longitudinal resolution in a biological tissue of 1.3 μm, 1.2 μm and 1.1 μm by using picosecond continuum light at center wavelengths of 1.06 μm, 1.31 μm and 1.55 μm, respectively.

Keywords: Photonic Crystal Fibers (PCFs); Finite Difference Method; Chromatic Dispersion; Supercontinuum Spectrum; Optical Coherence Tomography

1. INTRODUCTION

Photonic crystal fibers (PCFs) are new class of optical waveguide in recent years. PCF consists of a thread of silica with a lattice of microscopic air capillaries running along the entire length of the fiber. The design freedom of photonic crystal fibers (PCFs) can be used to tailor and extend the range of optical parameters like dispersion and nonlinearity [1]. Owing to the high index difference between silica core and air hole cladding, PCFs allow much stronger mode confinement, and thereby much higher nonlinearities. The reduced effective area A_{eff} is achieved by stronger mode confinement in the core with small core diameter, as a result nonlinearity γ can be increased. From the nonlinearity equation $\gamma = 2\pi n/\lambda A_{eff}$, it is clearly shown that nonlinearity is inversely proportional to the fiber's effective area. The zero dispersion wavelengths can thus be shifted toward the visible to near IR and matched with the operating wavelength of a large variety of nanosecond to femtosecond high peak power lasers, yielding broadband continuum [2]. The broadband supercontinuum (SC) generation in optical fibers currently attracts a lot of attention because of the high potential for applications in the fields of the optical communications, optical coherence tomography (OCT), optical metrology, time resolved absorption and spectroscopy [3-7]. OCT enables micron-scale, cross--sectional and three-dimensional imaging of biological tissues *in situ* and in real time. Ultrahigh-resolution OCT imaging in the spectral region from 1.0 to 1.6 μm requires extremely broad bandwidths because coherence length depends on the longitudinal resolution. However, this spectral region is of particular interest for OCT because it penetrates deeply into biological tissue and permits spectrally resolved imaging of water absorption bands. In this spectral region, attenuation is minimum due to absorption and scattering. It should be noted that scattering decreases at longer wavelengths in proportion to $1/\lambda^4$, indicating that the scattering magnitude at 1.0 μm - 1.6 μm wavelengths is lower than at the visible wavelengths [8]. Superluminescent diodes (SLDs) are often used for OCT imaging and typically have 10 - 15 μm longitudinal resolution [9]. This resolution is insufficient for identifying individual cells or assessing subcellular structures such as nuclei. Ultrahigh-resolution OCT in biological tissue, achieving high longitudinal resolution at center wavelength near 1.0 μm [10-12], 1.3 μm [13,14] and 1.55 μm [15], has been demonstrated with femtosecond lasers as low coherence light sources. On the other hand, telecommunication window (around 1.55 μm) is the most attractive window in optical communication systems, dispersion compensation and nonlinear optics because of the minimum transmission loss of the fiber. Chromatic dispersion controlling and simultaneously keeping the confinement loss to a level below

the Rayleigh scattering limit in conventional fiber is very important for any optical systems. Recently, we have reported that it is possible to achieve broad supercontinum spectrum, high longitudinal resolution in biological tissue by using HN-PCF with ultraflattened chromatic dispersion properties [16].

Therefore, as part of the ongoing efforts in pursuit of simple structures in PCFs for SCG light sources, in this paper, we further demonstrate an HN-PCF with an ultra-flattened chromatic dispersion over a wider wavelength range, broad supercontinum spectrum, and high longitudinal resolution. In this paper, we explore the possibility of generating supercontinuum spectrum by using pico-second pulses in six-ringed highly nonlinear photonic crystal fiber (HN-PCF) ultrahigh-resolution OCT and optical transmission systems. The three different sizes air hole diameters are used in order to simplify the structure and decrease the fabrication difficulties. From numerical simulation results we achieve very high non-linear coefficients with ultra-flattened chromatic dis-persion, low dispersion slope, broadband SC spectrum, ultra-high resolution, high power and low confinement loss, simultaneously. We realize longitudinal resolution in biological tissue of 1.3 μm, 1.2 μm and 1.1 μm at the center wavelengths of 1.06 μm, 1.31 μm and 1.55 μm for the application of OCT system. This is, to our knowl-edge, the highest resolution achieved to date for bio-logical imaging in these wavelengths. Moreover, pico-second pulse laser source is cheaper than that of femto-second laser source in this case it attracts in practical implementation.

2. GEOMETRY OF THE PROPOSED HN-PCF

Figure 1(a) shows the transverse geometry of hex-agonal PCF (H-PCF). For the purpose of simplicity only two rings are shown. The air holes are arranged with a hexagonal symmetry across the cross section where Λ is the center-to-center spacing between the air holes, d is the air hole diameter, and the core diameter is $2a$. The H-PCF is constructed by repeating the unit equal lateral triangular lattice with vertex angle of 60˚ shown in **Fig-ure 1(b)**. The air holes of diameter d are located at each corner of the equilateral triangle. A cross-section of the proposed HN-PCF structure is illustrated in **Figure 1(c)**. In this design, first ring air hole diameter is d_1, second and third ring air hole diameter is d_2, fourth to sixth ring air hole diameter is d. PCFs possess artificially-periodic cladding consisting of micrometer-sized air holes allow flexible tailoring of the dispersion curves. As a conse-quence we need to incorporate much more sophisticated structure with more degrees of freedom regarding the total number of design parameters in order to achieve

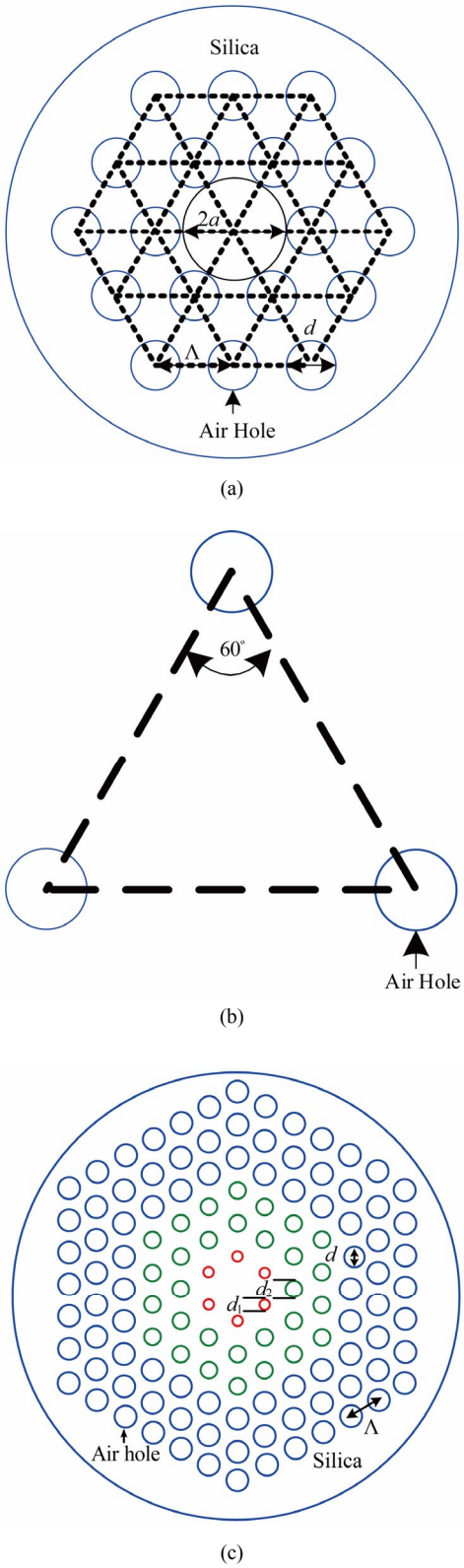

Figure 1. Transverse geometry of the H-PCF: (a) Structure with two rings and (b) a unit equal lateral triangular lattice and (c) Geometry of the proposed six ring HN-PCF.

flat dispersion, small effective area, while keeping the confinement losses as low as possible. For index-guiding PCFs as periodic lattice arrangement for the air holes are not absolutely necessary to achieve guidance of light in the core region [3]. The proposed HN-PCF is designed following this principle to control the dispersion and dispersion slope in wide wavelength range. Therefore, in the proposed structure, we break the uniformity of the cladding region and the diameter of the first ring air hole is reduced to d_1 to obtain near zero flat dispersion, while the diameter of other air hole rings d is selected large for keeping low confinement loss value.

3. NUMERICAL SIMULATION METHOD

The full-vector finite difference method (FDM) [17,18] with anisotropic perfectly matched boundary layers (PMLs) is used to calculate the different properties of PCFs. Anisotropic PMLs absorbing boundary are positioned outside the outermost ring of air holes in order to reduce the simulation window and to evaluate the confinement loss of the proposed fiber with a finite number of air hole rings. The material dispersion given by Sellmeier equation is directly included in the calculation. Therefore, chromatic dispersion in References [17,18] corresponds to the total dispersion of the PCFs. Chromatic dispersion is an important phenomenon in the propagation of short pulses in optical fibers. Temporally short pulses have a large spectral bandwidth. The different spectral components of the pulse travel through the medium at slightly different group velocities because of chromatic dispersion, which can result in a temporal broadening of the light pulses with no effect on their spectral compositions. Once the modal effective indices is obtained by solving an eigenvalue problem drawn from the Maxwell's equations using the FDM, the parameter chromatic dispersion, confinement loss and effective area can be calculated by [17,18]

$$D(\lambda)=\frac{\mathrm{d}}{\mathrm{d}\lambda}\left(\frac{1}{v_g}\right)=-\frac{2\pi c}{\lambda^2}\beta_2=-\frac{\lambda}{c}\frac{\mathrm{d}^2\,\mathrm{Re}\left(n_{eff}\right)}{\mathrm{d}\lambda^2} \quad (1)$$

where, v_g is group velocity, β_2 is group velocity dispersion, λ is the wavelength, c is the velocity of light in vacuum, Re(n_{eff}) is the real part of n_{eff}.

$$L_c=-20\log_{10}\mathrm{e}^{-k_0\,\mathrm{Im}\left(n_{eff}\right)}=8.686k_0\,\mathrm{Im}\left(n_{eff}\right) \quad (2)$$

where, Im(n_{eff}) is the imaginary part of n_{eff}, $k_0 = 2\pi/\lambda$ is the free space wave number.

$$A_{eff}(\lambda)=\frac{\left[\iint\left(\left|E_x(x,y)\right|^2+\left|E_y(x,y)\right|^2\right)\mathrm{d}x\mathrm{d}y\right]^2}{\iint\left(\left|E_x(x,y)\right|^2+\left|E_y(x,y)\right|^2\right)^2\mathrm{d}x\mathrm{d}y} \quad (3)$$

where, E is the transverse electric field derived by solving Maxwell's equations. We can know that the effective area depends on two factors: the refractive index difference between the cores and the cladding, the dimension of the cores.

Since amorphous silica can be treated as a homogeneous material, the lowest-order nonlinear coefficient is the third-order susceptibility $\chi^{(3)}$ [8]. Most of the nonlinear effects in optical fibers therefore originate from nonlinear refraction, a phenomenon that refers to the intensity dependence of the refractive index resulting from the contribution of $\chi^{(3)}$, *i.e.*, the refractive index of the fiber becomes

$$n=n_1+n_2\left|E\right|^2 \quad (4)$$

where n_1 is the linear part, $\left|E^2\right|$ is the optical intensity inside the fiber, n_2 is the nonlinear refractive index related to $\chi^{(3)}$ by the following relation

$$n_2=\frac{3}{8n_1}\mathrm{Re}\left(\chi^{(3)}_{xxxx}\right) \quad (5)$$

where Re stands for the real part. Nonlinear coefficient is calculated with following equation [8].

$$\gamma=\left(\frac{\omega}{c}\right)\left(\frac{n_2}{A_{eff}}\right)=\left(\frac{2\pi}{\lambda}\right)\left(\frac{n_2}{A_{eff}}\right) \quad (6)$$

where γ is the nonlinear coefficient, ω is the angular frequency, n_2 is the nonlinear refractive index, λ is the wavelength of the light, (n_2/A_{eff}) is the nonlinear constant. Two ways to enhance the nonlinearity is to reduce the effective area through a smaller core diameter and higher index contrast. By appropriate choice of size and pattern of PCF section, the effective area can be reduced; thereby the nonlinearity of the fiber can be increased by increasing the intensity inside the fiber which increases the nonlinear phase change during propagation.

4. RESULTS AND DISCUSSION

The wavelength dependence properties of chromatic dispersion, dispersion slope, effective area, nonlinear coefficient and confinement loss for the six-ring HN-PCF in **Figure 1(c)** are shown in **Figure 2**, where center-to-center spacing Λ = 0.87 μm, the relative sizes of air holes are d_1 = 0.33 μm, d_2 = 0.78 μm, d = 0.84 μm. The proposed HN-PCF show ultra-flattened chromatic dispersion of 0 ± 4.0 ps/(nm·km) is from 1.06 to 1.68 μm wavelength range (620 nm band). The chromatic dispersion slopes variation is 0 ± 0.04 ps/(nm^2·km) in expected wavelength range. In OCT window, the effective area of the HN-PCF is 1.78 μm^2 and 2.1 μm^2 at 1.06 μm and 1.31 μm, respectively. And the corresponding nonlinear coefficients are more than 102.0 [Wkm]$^{-1}$ and

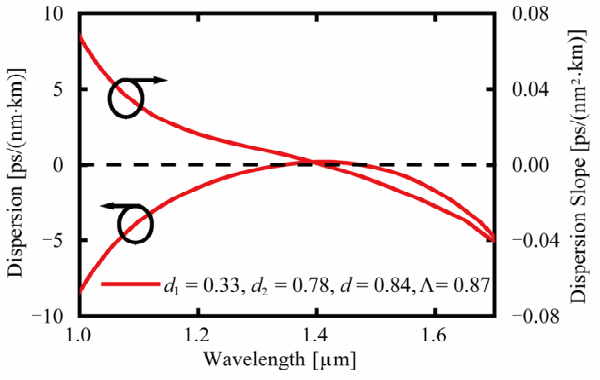

(a)

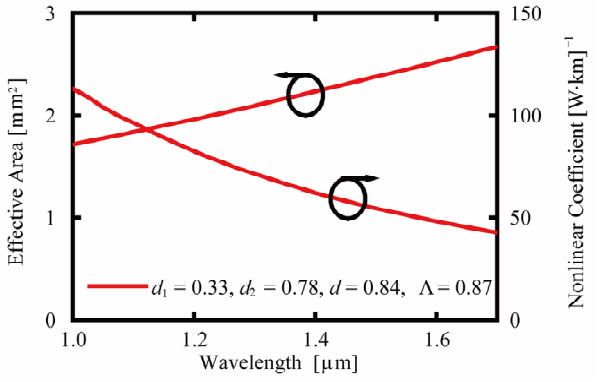

(b)

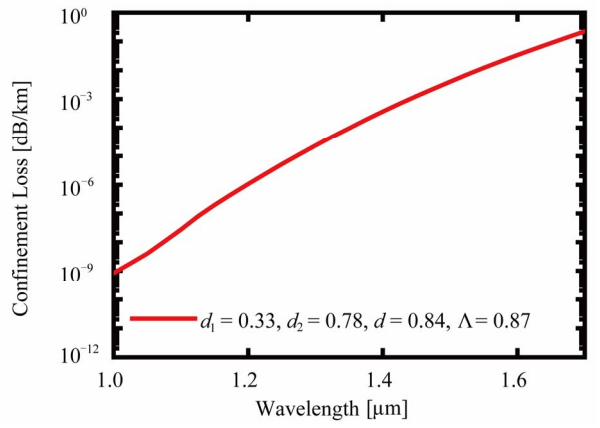

(c)

Figure 2. (a) Chromatic dispersion and dispersion slope, (b) Effective area and nonlinear coefficient and (c) Confinement loss characteristics.

70.0 [Wkm]$^{-1}$ at 1.06 μm and 1.31 μm, respectively. On the other hand, in telecommunication window, the effective area of the proposed HN-PCF is 2.45 μm^2 at 1.55 μm and the corresponding nonlinear coefficients are more than 51.0 [Wkm]$^{-1}$. These nonlinear coefficients values are higher than those ones reported in References [2-4,11, 12,17]. The confinement losses are less than 10^{-1} dB/km in the targeted wavelength range which is lower than Rayleigh scattering loss in conventional fiber [8].

For numerical calculation of SC spectra, the nonlinear Schrödinger equation (NLSE) is used and this NLSE is solved by using split-step Fourier method [8].

$$\frac{\partial A}{\partial Z} + \frac{\alpha}{2}A + \frac{i}{2}\beta_2\frac{\partial^2 A}{\partial T^2} - \frac{1}{6}\beta_3\frac{\partial^3 A}{\partial T^3} = i\gamma\left[|A|^2 A + i\frac{\lambda_c}{2\pi c}\frac{\partial}{\partial T}\left(|A|^2 A\right) - T_R A\frac{\partial |A|^2}{\partial T}\right] \quad (7)$$

where A is the complex amplitude of the optical field, α is the attenuation constant of the fiber, β_i (i =1 to 3) are the i-th order of the Taylor series expansion of the propagation constant around the carrier frequency, γ is the nonlinear coefficient, λ_c is the center wavelength, and T_R is the Raman scattering parameter, respectively.

SC generation in the proposed HN-PCF is numerically calculated which is shown in **Figures 3(a)**, **(b)** and **(c)**. In **Figure 3**, we consider the propagation of the sech^2 waveform with the full width at half maximum (FWHM) T_{FWHM} and the Raman scattering parameters T_R are 1.0 ps and 3.0 fs, respectively, through the proposed HN-PCF. The input power P_{in} of the incident pulse are 43.0 W, 8.0 W and 40.0 W, at center wavelength λ_c of 1.06 μm, 1.31 μm and 1.55 μm, respectively. Calculated β_2 and β_3 values are shown in table 1 for the center wavelength 1.06 μm, 1.31 μm and 1.55 μm. From **Table 1**, it is observed that β_2 value at 1.31 μm wavelength is lower than that of 1.06 μm and 1.55 μm wavelengths. If we increase incident power at 1.31 μm wavelength, then would need to increase β_2 value as well. However, in our calculation we found β_2 value of this fiber to be 0.23 [ps^2/km] at the 1.31 μm wavelength. Moreover, it is seen that broad FWHM of SC spectrum and short fiber length L_F is achieved at center wavelength λ_c = 1.55 μm and λ_c = 1.06 μm, respectively.

If a Gaussian source line shape is assumed, then the coherence length l_c of an OCT system is given by [12]. This l_c is very important for estimating the longitudinal resolution l_r in air and biological tissue. After calculating l_c, longitudinal resolution in air and biological tissue can be estimated [12]. For ultrahigh-resolution OCT imaging l_c should be low value because l_r is proportional with l_c.

$$l_c = \frac{2\ln 2}{\pi}\frac{\lambda_c^2}{\Delta\lambda} \quad (8)$$

$$l_r = \frac{l_c}{n_{tissue}} \quad (9)$$

where λ_c is the center wavelength and $\Delta\lambda$ is the FWHM spectral width, n_{tissue} is the refractive index of the biological tissue.

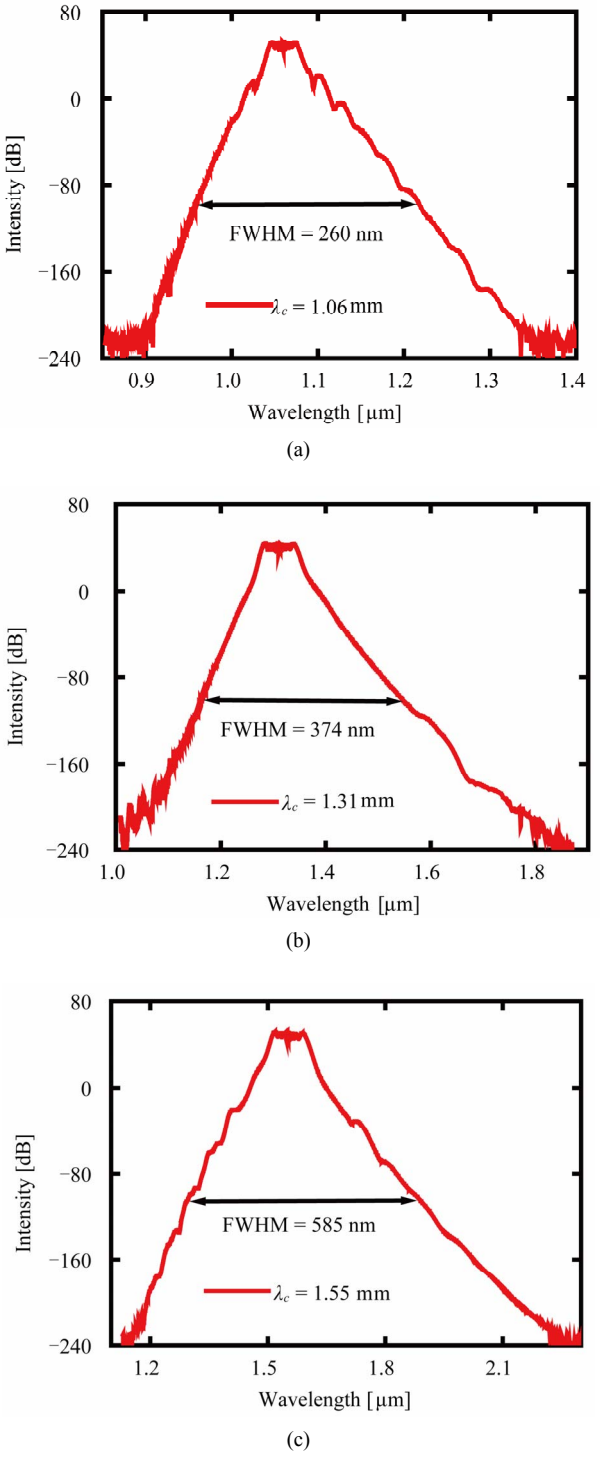

Figure 3. Intensity spectrum of the proposed HN-PCF at (a) 1.06 μm, (b) 1.31 μm and (c) 1.55 μm.

For ultrahigh-resolution OCT imaging l_c should be low value because l_r is proportional with l_c. The calculated l_c and l_r values are shown in table 1 when typical n_{tissue} is 1.44 at 1.06 μm, and 1.65 at 1.31 μm and 1.55 μm, respectively [19]. These calculated l_r values are lower than that of reported in References [5,9,10,13-15]. From the calculated data of **Table 1**, it is found that among three center wavelengths, the highest resolution is obtained at 1.55 μm wavelength.

Figures 4 (a), **(b)** and **(c)** represents the intensity spectra of the proposed HN-PCF at center wavelengths 1.06, 1.31 and 1.55 μm, respectively in different input powers. From these figures, it is seen that intensity spectra are gradually broadening with increasing the input power, P_{in} at the particular wavelength.

The wavelength dependence of chromatic dispersion variation after changing air hole diameter d_1 and d_2 for the HN-PCF in **Figure 1(c)** is depicted in **Figures 5 (a)** and **(b)**, respectively. It is reported that the air hole diameter of the first ring is particularly important for the overall dispersion flatness [20] and it may vary within ± 1% during the fabrication process [21]. To take this matter into consideration, the air hole diameter d_1 of the first ring is varied up to ± 5% from the optimum value as can be shown in **Figure 5(a)**. From the **Figure 5(a)** results, it is found that the chromatic dispersion remains unchanged until ±4% variation of the diameter d_1. In **Figure 5(a)**, it is observed that chromatic dispersion curves shift downward and upward from the optimum one in +5% and −5% variation of d_1, respectively, in longer wavelengths. On the other hand, from **Figure 5(b)**, it is depicted that after changing air hole diameter d_2 at 0.84 μm value, the chromatic dispersion curve is shifted upward from the optimum curve. From this result, it is confirmed that air hole diameter d_2 is very important to obtain the optimum result. Hence, it is crucial to select air hole diameter d_2 value very carefully.

5. CONCLUSIONS

We have proposed broadband SC generating phonic crystal fiber as a light source for ultrahigh-resolution OCT imaging system by using picosecond pulses. We

Table 1. Calculated coherence lengths and longitudinal resolutions.

Paramters	λ_c = 1.06 [μm]	λ_c = 1.31 [μm]	λ_c = 1.55 [μm]
β_2 [ps^2/km]	2.98	0.23	1.01
β_3 [ps^3/km	0.01	0.0	−0.01
T_R [fs]	3.0	3.0	3.0
P_{in} [W]	43.0	8.0	40.0
L_F [m]	7.0	70.0	18.0
FWHM [nm]	260.0	374.0	585.0
l_c [μm]	1.9	2.0	1.8
l_r [μm]	1.3	1.2	1.1

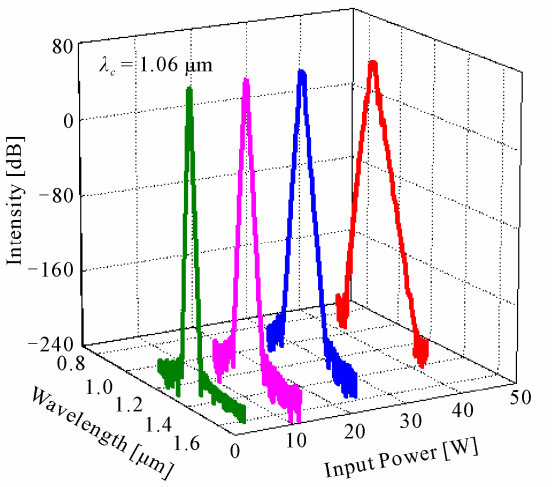

(a)

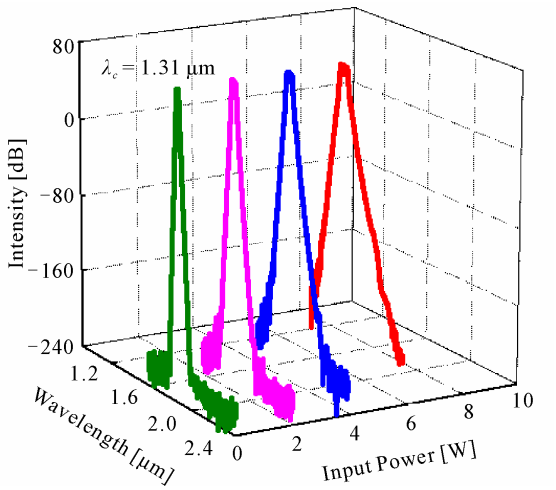

(b)

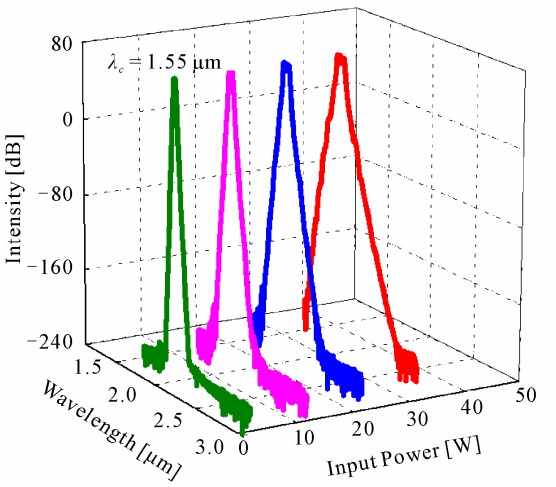

(c)

Figure 4. Intensity spectrum at center wavelength (a) 1.06 μm, (b) 1.31 μm and (c) 1.55 μm of the proposed HN-PCF in different input powers.

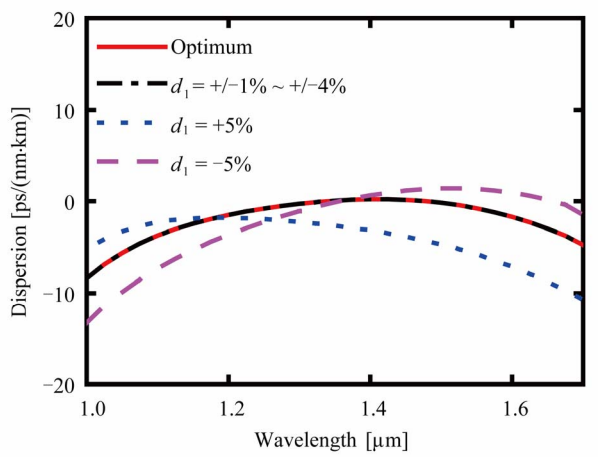

(a)

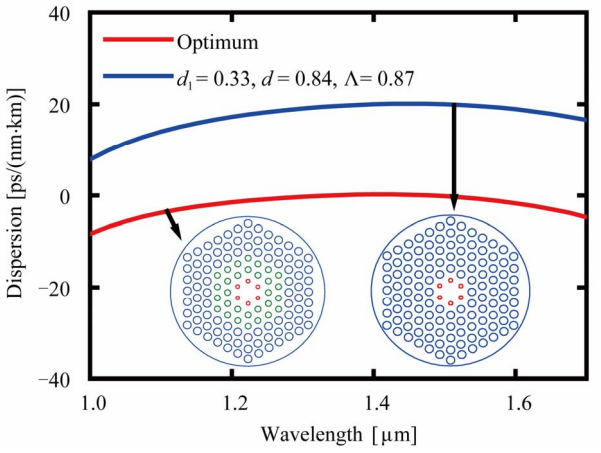

(b)

Figure 5. (a) Plot of chromatic dispersion tolerances and (b) Chromatic dispersion properties after changing the air hole diameter of second and third rings of the proposed HN-PCF.

achieved high longitudinal resolution in a biological tissue of 1.3 μm, 1.2 μm and 1.1 μm at center wavelength of 1.06, 1.31 and 1.55 μm, respectively. From numerical simulation results, it was found that the proposed HN-PCF exhibits high nonlinear coefficients with ultra-flattened chromatic dispersion, low dispersion slopes, broadband SC spectrum, ultra-high resolution, high power and very low confinement losses, simultaneously. The broad SC bandwidth of the light source will permit in both high resolution and improve the diagnosis of diseases from 1.0 to 1.6 μm wavelength ranges. The design procedure of the proposed HN-PCF structure could be more efficient and easier because for optimization relatively fewer geometrical parameters are needed. Moreover, it should be noted that the picosecond light source is relatively cheaper; hence, the proposed HN-PCF would be useful in practical applications. Such

broadband supercontinuum generated HN-PCF will be useful in the precise measurement of optical frequencies, high resolution noninvasive medical imaging (optical coherence tomography), atomic spectroscopy and telecommunication dense wavelength division multiplexing.

6. ACKNOWLEDGEMENTS

Authors gratefully acknowledge to the Japan Society for Promotion of Science (JSPS) for their support in carrying out this research work, JSPS ID number P 09078. Dr. Feroza Begum is a JSPS research fellow.

REFERENCES

[1] Russel, P.St.J. (2003) Photonic crystal fibers. *Science*, **299**, 358-362. doi:10.1126/science.1079280

[2] Champert, P.-A., Couderc, V., Leproux, P., Février, S., Tombelaine, V., Labonté, L., Roy, P., Froehly, C. and Nérin, P. (2004) White-light supercontinuum generation in normally dispersive optical fiber using original multi-wavelength pumping system. *Optics Express*, **12**, 4366-4371. doi:10.1364/OPEX.12.004366

[3] Saitoh, K. and Koshiba, M. (2004) Highly nonlinear dispersion-flattened photonic crystal fibers for supercontinuum generation in a telecommuinication window. *Optics Express*, **12**, 2027-2032. doi:10.1364/OPEX.12.002027

[4] Yamamoto, T., Kubota, H., Kawanishi, S., Tanaka, M. and Yamaguchi, S. (2003) Supercontinuum generation at 1.55 μm in a dispersion-flattened polarization-maintaining photonic crystal fiber. *Optics Express*, **11**, 1537-1540. doi:10.1364/OE.11.001537

[5] Hartl, I., Li, X.D., Chudoba, C., Ghanta, R.K., Ko, T.H., Fujimoto, J.G., Ranka, J.K. and Windeler, R.S. (2001) Ultrahigh-resolution optical coherence tomography using continuum generation in an air-silica microstructure optical fiber. *Optics Letters*, **26**, 608-610. doi:10.1364/OL.26.000608

[6] Sotobayashi, H., Chujo, W. and Kitayama, K. (2002) Photonic gateway: multiplexing formate conversions of OCDM-to-WDM and WDM-to-OCDM at 40 Gb/s (4 × 10 Gb/s). *Journal of Lightwave Technology*, **20**, 2022-2028. doi:10.1109/JLT.2002.806769

[7] He, G.S., Lin, T.C., Prasad, P.N., Kannan, R., Vaia, R.A. and Tan, L.-S. (2002) New technic for degenerated two-photon absorption spectral measurements using femtosecond continuum generation. *Optics Express*, **10**, 566-574.

[8] Agrawal, G.P. (1995). Nonlinear fiber optics. Academic Press, San Diego.

[9] Youngquist, R.C., Carr, S. and Davies, D.E.N. (1987) Optical coherence-domain reflectometry: A new optical evaluation technique. *Optics Letters*, **12**, 158-160. doi:10.1364/OL.12.000158

[10] Lim, H., Jiang, Y., Wang, Y., Huang, Y.-C., Chen, Z. and Wise, F.W. (2005) Ultrahigh-resolution optical coherence tomography with a fiber laser source at 1 μm. *Optics Letters*, **30**, 1171-1173. doi:10.1364/OL.30.001171

[11] Tse, M.L.V., Horak, P., Poletti, F., Broderick, N.G.R., Price, J.H.V., Hayes, J.R. and Richardson, D.J. (2006) Supercontinuum generation at 1.06 μm in holey fibers with dispersion flattened profiles. *Optics Express*, **14**, 4445- 4451. doi:10.1364/OE.14.004445

[12] Kinjo, T., Namihira, Y., Arakaki, K., Koga, T., Kaijage, S.F., Razzak, S.M.A., Begum, F., Nozaki, S. and Higa, H. (2010) Design of highly nonlinear dispersion-flattened square photonic crystal fiber for medical applications. *Optics Review*, **17**, 61-65. doi:10.1007/s10043-010-0011-x

[13] Colston, B.W., Jr., Sathyam, U.S., DaSilva, L.B., Everett, M.J., Stroeve, P. and Otis, L.L. (1998) Dental OCT. *Optics Express*, **3**, 230-238. doi:10.1364/OE.3.000230

[14] Boppart, S.A., Bouma, B.E., Pitris, C., Southern, J.F., Brezinski, M.E. and Fujimoto, J.G. (1998) *In vivo* cellular optical coherence tomography imaging. *Nature Medicine*, **4**, 861-865. doi:10.1038/nm0798-861

[15] Lee, J.H., Jung, E.J. and Kim, C.-S. (2009) Incoherent, CW supercontinuum source based on Erbium fiber ASE for optical coherence tomography imaging. *Proceedings of OptoEelectronics and Communication Conference*, Hong- kong, 13-17 July 2009, 1-2.

[16] Begum, F., Namihira, Y., Kinjo, T. and Kaijage, S. (2010) Supercontinuum generation in photonic crystal fibers at 1.06, 1.31 and 1.55 μm wavelengths. *Electronics Letter*, **46**, 1518-1520. doi:10.1049/el.2010.2133

[17] Begum, F., Namihira, Y., Kaijage, S., Razzak, S.M.A., Hai, N.H., Kinjo, T., Miyagi, K. and Zou, N. (2009) Design and analysis of novel highly nonlinear photonic crystal fibers with ultra-flattened chromatic dispersion. *Optics communications*, **282**, 1416-1421. doi:10.1016/j.optcom.2008.12.005

[18] Shen, L.-P., Huang, W.-P. and Jian, S.-S. (2003) Design of photonic crystal fibers for dispersion-related applications. *Journal of Lightwave Technology*, **21**, 1644-1651. doi:10.1109/JLT.2003.814397

[19] Ohmi, M., Ohnishi, Y., Yoden, K. and Haruna, M. (2000) In vitro simultaneous measurement of refractive index and thickness of biological tissue by the low coherence interferometry. *IEEE Transactions on Biomedical Engineering*, **47**, 1266-1270. doi:10.1109/10.867961

[20] Reeves, W.H., Knight, J.C., Russell, P.St.J. and Roberts, P.J. (2002) Demonstration of ultra-flattened dispersion in photonic crystal fibers. *Optics Express*, **10**, 609-613.

[21] Poletti, F., Finazzi, V., Monro, T.M., Broderick, N.G.R., Tse, V. and Richardson, D.J. (2005) Inverse design and fabrication tolarences of ultra-flattened dispersion holey fibers. *Optics Express*, **13**, 3728-3736. doi:10.1364/OPEX.13.003728